NASA TECHNICAL NOTE

NASA TN D-8263
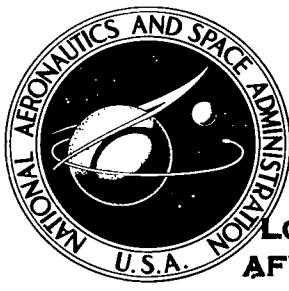
ANALYTICAL COMPARISON OF EFFECTS
OF SOLID-FRICTION AND VISCOUS
STRUCTURAL DAMPING ON PANEL FLUTTER

Herbert J. Cunningham

Langley Research Center
Hampton, Va. 23665
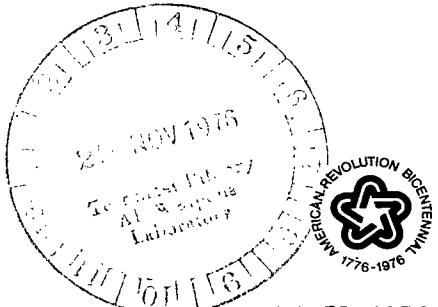
1. Report No. NASA TN D-8263	2. Government Accession No.	3. Recipient's Catalog No.
4. Title and Subtitle ANALYTICAL COMPARISON OF EFFECTS OF SOLID-FRICTION AND VISCOUS STRUCTURAL DAMPING ON PANEL FLUTTER		5. Report Date November 1976
		6. Performing Organization Code
7. Author(s) Herbert J. Cunningham		8. Performing Organization Report No. L-10914
9. Performing Organization Name and Address NASA Langley Research Center Hampton, VA 23665		10. Work Unit No. 505-02-21-01
		11. Contract or Grant No.
12. Sponsoring Agency Name and Address National Aeronautics and Space Administration Washington, DC 20546		13. Type of Report and Period Covered Technical Note
		14. Sponsoring Agency Code

15. Supplementary Notes

16. Abstract

A Galerkin modal analysis is presented that accounts for the effects of both solid-friction and viscous structural damping on panel flutter, based on unsteady aerodynamic forces from supersonic potential flow. The eigensolutions are made by complex eigenvalue computer routines.

Markedly different effects on the flutter boundary of the two types of structural damping are obtained. This result establishes that there is not, in general, an "equivalent viscous" damping for solid-friction damping.

For the limiting case of the static-aerodynamic approximation, a substantially different flutter dynamic pressure is obtained for solid friction identically zero compared with solid friction approaching zero as a limit. Use of the quasi-static aerodynamic approximation eliminates that difference.

17. Key Words (Suggested by Author(s)) Flutter Panel flutter Aeroelasticity Structural damping Hysteresis damping Viscous damping		18. Distribution Statement Unclassified – Unlimited Subject Category 39	
19. Security Classif. (of this report) Unclassified	20. Security Classif. (of this page) Unclassified	21. No. of Pages 35	22. Price* $3.75

ANALYTICAL COMPARISON OF EFFECTS OF SOLID-FRICTION
AND VISCOUS STRUCTURAL DAMPING ON PANEL FLUTTER

Herbert J. Cunningham
Langley Research Center

SUMMARY

A Galerkin modal analysis is presented that accounts for the effects of both solid-friction and viscous structural damping on panel flutter, based on unsteady aerodynamic forces from supersonic potential flow. The eigensolutions are made by complex eigenvalue computer routines.

Markedly different effects on the flutter boundary of the two types of structural damping are obtained. This result establishes that there is not, in general, an "equivalent viscous" damping for solid-friction damping.

For the limiting case of the static-aerodynamic approximation, a substantially different flutter dynamic pressure is obtained for solid friction identically zero compared with solid friction approaching zero as a limit. Use of the quasi-static aerodynamic approximation eliminates that difference.

INTRODUCTION

Two representations of structural damping have been used in published panel-flutter analyses. The two types or representations are: (1) solid friction that is termed "hysteretic" in some of the literature and is accounted for within a complex stiffness; and (2) the viscous type, that for harmonic motion is also characterized by a hysteresis loop in stress-strain and load-deflection plots.

Neumark in reference 1 has provided a thorough and careful analysis of the basic characteristics of viscous and solid-friction (hysteretic) damping for single-degree-of-freedom systems in free and forced oscillation; his findings apply as well to multiple-degree-of-freedom systems oscillating in a single simple harmonic motion. Perhaps the earliest application of viscous-type structural damping to panel-flutter analysis appears in reference 2. The model analyzed was an infinite streamwise array of panels with a continuous spectrum of traveling-wave modes, and some ranges of parameters were found for which added damping was destabilizing.

Reference 3 included an early application to panel-flutter analysis of the solid-friction type of structural damping used in wing-flutter analysis in reference 4. Added

damping was found to be stabilizing in some parameter areas but destabilizing in others. An analysis is given in reference 5 of plane panels subjected to in-plane loading, linear piston-theory aerodynamics, and with solid-friction (hysteresis) damping both in bending and in longitudinal compression. The destabilizing effect of structural damping for some ranges of parameters was found also for this case. Reference 5 is notable for its comprehensive list of references (69).

The extensive investigation of reference 6 included some consideration of viscous-type structural damping and found that it had a moderate destabilizing effect for some parameters, especially in the presence of low aerodynamic damping that accompanies low air density. A careful study is given in reference 7 of the effects of both viscous and hysteretic (solid-friction) damping on the flutter of a rectangular membrane. It was found that an increase of either or both types of damping is destabilizing, and that, for the same value of structural damping coefficient, viscous damping is more destabilizing than solid-friction (hysteretic) damping.

The purpose of the present report is to present two methods of solution for routine calculation of panel-flutter characteristics as affected by the two types of damping in the presence of the complete unsteady aerodynamic forces and to show the substantially contrasting effects of the two dampings. The present work is an outgrowth from that reported in reference 8 for unyawed panels. A yawed panel is analyzed herein to show the effects from the two dampings. In general, the complete unsteady aerodynamic forces from potential-flow theory are employed. The static and quasi-static aerodynamic approximations are also used for comparison purposes. The equations for the generalized aerodynamic forces are given in an appendix.

SYMBOLS

D flexural stiffness of panel, $\dfrac{Et^3}{12\left(1 - \nu^2\right)}$, where ν is Poisson's ratio and E is Young's modulus

g_{sf} modal-independent coefficient of solid-friction (sf) structural damping (eq. (12c))

$g_{i,sf}, g_{j,sf}$ coefficients of solid-friction (sf) structural damping for modes i and j, respectively

$\bar{g}_{j,sf}$ $= g_{j,sf} + g_{sf}$

$\bar{g}_{sf}$ $\bar{g}_{j,sf}$ before being specialized to mode j

$g_{i,v}, g_{j,v}, g_{B,v}$ coefficients of viscous (v) structural damping for modes i, j, and B, respectively, where B denotes any base or reference mode

G_s viscous structural damping constant (eq. (1))

$h_j \equiv h_j(\bar{x}, \bar{y})$ mode-shape deflection for mode j

$H_j(\bar{x}, \bar{y}, \tau)$ mode-j component in deflection z (eq. (5))

i unit of imaginaries, $\sqrt{-1}$

k reduced frequency based on reference length ℓ, $\omega \ell / V$

$K_{1,1}^{*}$ nondimensional eigenvalue quantity for fundamental panel mode (see eq. (19))

ℓ panel length at zero yaw

m_A mass of panel per unit surface area

M Mach number of undisturbed stream

M_i generalized mass for mode i (eq. (12))

M_0 value of M_i for $h_i = 1.0$; for uniform panels, $M_0 = m_A \ell w$

p, q number of half-waves lengthwise and widthwise, respectively, in panel modes h_j

Δp perturbation pressure difference on panel, positive with z

Δp_j complex amplitude of Δp for mode j (see eq. (8))

$\bar{q}_j(\tau), q_j$ time-varying generalized coordinate of motion for mode j and its complex amplitude, respectively, $\bar{q}_j(\tau) = e^{i\omega\tau} q_j$

$Q_{ij}, \bar{Q}_{ij}$ generalized aerodynamic-force elements, $\bar{Q}_{ij} = Q_{ij} \big/ (\rho V^2 \ell w)$ (eq. (11))

3

S	surface area of panel, region of integration
t	panel thickness
V	speed of undisturbed airstream
w	panel width at zero yaw
$\bar{x}, \bar{y}$	lengthwise and widthwise coordinates, based on ℓ and w, respectively, fixed to the panel as it yaws
z	z-coordinates of deflected panel surface
β	$= \sqrt{M^2 - 1}$
λ	dynamic-pressure parameter, $\rho V^2 \ell^3 \big/ \beta D$
Λ	angle of yaw of panel, deg
μ	ratio of panel mass to air mass, $\dfrac{m_A \ell w}{\rho \ell^2 w} = \dfrac{M_0}{\rho \ell^2 w} = \dfrac{m_A}{\rho \ell}$
ρ	density of undisturbed stream
τ	time
ω	circular frequency of motion
$\omega_i, \omega_j, \omega_B$	natural frequencies of panel modes i and j and of a chosen base or reference mode, respectively
ω^*	$= \omega \Big/ \sqrt{D \big/ \left(m_A \ell^4 \right)}$
Ω_f, Ω_s	flexibility and stiffness eigenvalues, respectively (eqs. (14) and (15))

4

ANALYSIS

Statement of the Problem

Figure 1 shows the yawed panel and its coordinate system. A minor difference from the analysis in reference 8 is that a right-hand coordinate system is used, so that here the z-axis is positive up. Correspondingly, deflections, downwashes, slopes, and forces have positive senses upward, but no signs in any of the equations need to be changed.

The usual assumptions are made of linear force-deflection relations, flow over only the upper surface, and no aerodynamic effects induced between top and bottom panel surfaces. No aerodynamic perturbation effects on the bottom surface of the panel are considered.

The governing differential equation of motion is that for a uniform isotropic panel with no in-plane loading. Two types of structural damping are accounted for: (1) the solid-friction mechanical hysteresis type, and (2) the viscous-structural type. The equation of equilibrium of forces is given as

$$D\nabla^4 z \left(1 + i\bar{g}_{sf}\right) + m_A \frac{\partial^2 z}{\partial \tau^2} + G_s \frac{\partial z}{\partial \tau} - \Delta p\left(\bar{x}, \bar{y}, \tau\right) = 0 \tag{1}$$

where the biharmonic operator is

$$\nabla^4 \equiv \frac{1}{\ell^4} \frac{\partial^4}{\partial \bar{x}^4} + \frac{2}{\ell^2 w^2} \frac{\partial^4}{\partial \bar{x}^2 \partial \bar{y}^2} + \frac{1}{w^4} \frac{\partial^4}{\partial \bar{y}^4} \tag{2}$$

and where D is the panel flexural stiffness, m_A is the panel mass per unit surface area, z is the deflection, τ is time, $\bar{g}_{sf}$ is a structural damping coefficient of the solid-friction (sf) type, G_s represents uniformly distributed panel viscous damping as introduced in reference 6, and Δp is the net perturbation pressure (positive with z) arising from the deflection and motion of the panel.

As explained in reference 6 the viscous damping constant G_s is expressed for any mode i as

$$G_s = g_{i,v} \omega_i m_A \tag{3}$$

where ω_i is the natural frequency of mode i and $g_{i,v}$ is a structural damping coefficient of the viscous (v) type. Furthermore, for G_s constant and independent of frequency, equation (3) implies that for any two modes i and j

5

$$g_{i,v}\omega_i = g_{j,v}\omega_j = g_{B,v}\omega_B \qquad . \qquad\qquad\qquad\text{(4)}$$

where subscript B denotes any chosen base or reference mode.

Direct solution of equation (1) is not feasible for the type of panel deflections and aerodynamic forces considered. Therefore, the panel deflection at the flutter condition is considered to be sufficiently well approximated by a linear combination of selected deflection modes. For simple harmonic motion the time and space variations are separated in the usual way

$$z(\bar{x},\bar{y},\tau) = Z(\bar{x},\bar{y})e^{i\omega\tau}$$

where ω is the circular frequency of motion, the shape distribution $Z(\bar{x},\bar{y})$ can be complex, and $i = \sqrt{-1}$ is the unit of imaginaries, not to be confused with the modal index i. This leads to

$$z(\bar{x},\bar{y},\tau) \approx \sum_j H_j(\bar{x},\bar{y},\tau)$$

$$H_j(\bar{x},\bar{y},\tau) = \bar{q}_j(\tau)h_j(\bar{x},\bar{y}) = q_j e^{i\omega\tau}h_j(\bar{x},\bar{y}) \qquad\qquad\qquad\text{(5)}$$

where q_j is the complex amplitude of the generalized coordinate of motion. When the deflection mode shapes h_j are known that satisfy both the appropriate boundary conditions and the differential equation (1), with aerodynamic and damping terms omitted, then

$$D\nabla^4 h_j e^{i\omega\tau} = -m_A \frac{\partial^2\left(e^{i\omega\tau}h_j\right)}{\partial\tau^2} = m_A \omega_j^2 h_j e^{i\omega\tau} \qquad\qquad\qquad\text{(6)}$$

where on the right-hand side ω takes on its eigenvalue ω_j, the normal-mode frequency associated with h_j. Thus, the elastic-restoring term $D\nabla^4 h_j$ is representable in terms of ω_j. Substitution of equation (5) into equation (1) and use of equations (3), (4), and (6) lead to the result

$$\sum_j \bar{q}_j h_j m_A\left[\omega_j^2\left(1 + i\bar{g}_{j,sf}\right) - \omega^2\left(1 - i\frac{\omega_B}{\omega}g_{B,v}\right)\right] - \Delta p(\bar{x},\bar{y},\tau) = 0 \qquad\qquad\text{(7)}$$

6

where $\bar{g}_{sf}$ has taken on its modal values $\bar{g}_{j,sf}$. The frequency ω and the coordinates $\bar{q}_j$ are unknown, and the perturbation pressure remains to be specified.

In keeping with the modal analysis the pressure Δp is also expressed in terms of a modal series; that is,

$$\Delta p\left(\bar{x},\bar{y},\tau\right) \approx \sum_j \frac{\bar{q}_j}{\ell} \Delta p_j\left(\bar{x},\bar{y}\right) = e^{i\omega\tau} \sum_j \frac{q_j}{\ell} \Delta p_j\left(\bar{x},\bar{y}\right) \tag{8}$$

where each $\Delta p_j\left(\bar{x},\bar{y}\right)$ is a complex distribution function.

The Galerkin method is chosen to form the flutter-stability equations. Accordingly, the terms of equation (7) are multiplied by a mode shape $h_i\left(\bar{x},\bar{y}\right)$ and the resulting products are integrated over the area of the panel. When the modal index i is made successively 1, 2, 3,... for all h_i employed, the result is a system of equations expressing equilibrium of energy for a condition of minimum total energy of the panel. For modes that are orthogonal with respect to the mass distribution m_A,

$$\iint\limits_S m_A h_i h_j \, d\bar{x} \, d\bar{y} = 0 \qquad\qquad (i \neq j) \tag{9}$$

each of the set of equilibrium equations is of the form

$$q_i\left[\omega_i^2\left(1 + i\bar{g}_{i,sf}\right) - \omega^2\left(1 - \frac{\omega_B}{\omega} g_{B,v}\right)\right] \ell w \iint\limits_S m_A h_i^2 \, d\bar{x} \, d\bar{y}$$

$$- \sum_j \frac{q_j}{\ell} \ell w \iint\limits_S \Delta p_j h_i \, d\bar{x} \, d\bar{y} = 0 \tag{10}$$

From the last term of equation (10)

$$\ell w \iint\limits_S \Delta p_j h_i \, d\bar{x} \, d\bar{y} \equiv Q_{ij} \tag{11}$$

which is the generalized aerodynamic-force (element) term. The procedures for obtaining Q_{ij} are described in the appendix.

Solution of the Flutter Determinant

For the numerical solutions herein, it has been assumed that the individual modes used in the analysis are orthogonal with respect to the mass distribution (no inertial coupling between modes), and that there is also no significant stiffness coupling between modes. Provision is made for investigating two types of structural damping: (1) solid-friction, structural-hysteresis damping characterized by a coefficient $\bar{g}_{j,sf}$, and (2) viscous-structural damping characterized by a coefficient $g_{j,v}$. From equations (10) and (11) the set of equations that express the dynamic equilibrium of motion is given as

$$\left[\omega_i^2\left(1 + i\bar{g}_{i,sf}\right) - \omega^2\left(1 - i\frac{\omega_B}{\omega}g_{B,v}\right)\right]q_i M_i - \sum_j \frac{q_j}{\ell}Q_{ij} = 0 \qquad (i = 1,2,\ldots) \qquad (12a)$$

where

$$M_i = \ell w \int_0^1 \int_0^1 m_A h_i^2 \, d\bar{x} \, d\bar{y} \qquad (12b)$$

and where $\bar{g}_{i,sf}$, as introduced in reference 8, is considered as made up of two parts; that is,

$$\bar{g}_{i,sf} = g_{i,sf} + g_{sf} \qquad (12c)$$

where $g_{i,sf}$ remains the assigned or measured value for mode i and g_{sf} is a modal-independent mathematical convenience that is an aid in interpreting eigensolutions.

Preliminary to a solution of equations (12a), they are each divided by M_i and a substitution for Q_{ij} is made. The result is

$$\left[\omega_i^2\left(1 + i\bar{g}_{i,sf}\right) - \omega^2\left(1 - i\frac{\omega_B}{\omega}g_{B,v}\right)\right]q_i - \frac{\rho V^2 w}{M_i}\sum_j q_j \bar{Q}_{ij} = 0 \qquad (i = 1,2,\ldots) \qquad (12d)$$

where

$$\bar{Q}_{ij} = Q_{ij}\Big/\left(\rho V^2 \ell w\right)$$

Two types of solutions of the flutter equations, one adapted to each of the two types of structural damping, are described in the following discussion.

8

The flexibility solution.- A type of solution like that in reference 8, that is suited to the presence of solid-friction structural damping only, is termed here the "flexibility solution" because the dominant eigenvalue is that of the most flexible mode — the one with the lowest of the frequencies ω_i. To obtain this solution based on equations (12) an asymptotic expression for $1 + i\bar{g}_{i,sf}$

$$1 + i\bar{g}_{i,sf} = 1 + ig_{i,sf} + ig_{sf} \sim \left(1 + ig_{i,sf}\right)\left(1 + ig_{sf}\right) \tag{13}$$

is substituted, $g_{B,v}$ is set equal to zero, and equation (12d) is multiplied by

$-\omega_B^2 \Big/ \left[\omega_i^2\omega^2\left(1 + ig_{i,sf}\right)\right]$. Thus,

$$\left[-\Omega_f + \left(\frac{\omega_B}{\omega_i}\right)^2 \Big/ \left(1 + ig_{i,sf}\right)\right]q_i + \left(\frac{\omega_B}{\omega_i}\right)^2 \frac{1/\mu}{1 + ig_{i,sf}} \frac{1}{k^2} \frac{M_0}{M_i} \sum_j q_j \bar{Q}_{ij} = 0 \qquad (i = 1,2,\ldots) \tag{14a}$$

where ω_B is a chosen base or reference frequency, the flexibility eigenvalue Ω_f is

$$\Omega_f \equiv \left(\frac{\omega_B}{\omega}\right)^2 \left(1 + ig_{sf}\right) \tag{14b}$$

$$\frac{1}{\mu} = \frac{\rho\ell^2 w}{m_A \ell w} = \frac{\rho\ell}{m_A} \tag{14c}$$

$$M_0 = m_A \ell w \tag{14d}$$

and $k \equiv \omega\ell/V$ is the reduced frequency. Note that $g_{i,sf}$ can be different for each mode i.

The stiffness solution.- A type of solution that is suited to analysis of the effects of viscous-structural damping, and can simultaneously account for the presence of solid-friction damping, is termed here the "stiffness solution" because the dominant eigenvalue is that of the stiffest mode — the one with the highest of the frequencies ω_i. To obtain this solution the modal-independent coefficient g_{sf} of equation (13) is dropped and equation (12d) is divided by ω_B^2. Thus,

$$\left[-\Omega_s + \left(\frac{\omega_i}{\omega_B}\right)^2 \left(1 + ig_{i,sf}\right)\right]q_i - \left(\frac{1}{\mu}\right)\left(\frac{\omega}{\omega_B}\right)^2 \frac{1}{k^2} \frac{M_0}{M_i} \sum_j q_j \bar{Q}_{ij} = 0 \qquad (i = 1,2,\ldots) \tag{15a}$$

obtained where the stiffness eigenvalue Ω_s is

$$\Omega_s \equiv \left(\frac{\omega}{\omega_B}\right)^2 \left(1 - i\frac{\omega_B}{\omega}g_{B,v}\right) \qquad (15b)$$

As in the flexibility solution $g_{i,sf}$ can be different for each mode i. The eigenvalues appear only on the principal diagonal and are readily calculated by an eigenvalue computer subroutine.

Solution techniques.- With aerodynamic forces derived from unsteady potential flow, flutter boundaries cannot be calculated directly or explicitly. A search technique must be employed, and this is illustrated for a case with the following panel and flow parameters: simply supported edges, $\ell/w = \sqrt{0.3}$, $\Lambda = 10^{\circ}$, two assumed natural beam modes in both length and width directions, $g_{i,sf} = 0$, $M = 3.0$, and $k = 0.25$. Equations (14) for the flexibility solution and equations (15) for the stiffness solution are solved by using standard complex-eigenvalue computer routines, since the eigenvalues Ω_f and Ω_s appear only on the main diagonal.

For an initial assumption of $1/\mu = 0$ the eigenvalues are those for the assumed modes in a vacuum. The results are the points at the "foot" of each curve (i.e., at $\lambda = 0$ and $1/\mu = 0$) in all the parts of figure 2(a) from the flexibility solution and of 2(b) from the stiffness solution. The labeled values of p,q are the number of half-waves in each assumed mode lengthwise (p), and widthwise (q). As $1/\mu$ is monotonically increased the traces that are plotted are ω^* and g_{sf} $\left(\text{or } g_{B,v}\right)$ against λ on the left, and stiffness parameter and g_{sf} $\left(\text{or } g_{B,v}\right)$ against $1/\mu$ on the right. The frequency ratio ω/ω_B and g_{sf} $\left(\text{or } g_{B,v}\right)$ are obtained from the eigenvalues. The dimensionless frequency parameter ω^* $\left(\text{and } \omega_B^* \text{ and } \omega_i^*\right)$ are defined by

$$\begin{Bmatrix} \omega^* \\ \omega_B^* \\ \omega_i^* \end{Bmatrix} \equiv \frac{1}{\sqrt{\dfrac{D}{m_A \ell^4}}} \begin{Bmatrix} \omega \\ \omega_B \\ \omega_i \end{Bmatrix} \qquad (16)$$

(see appendix A of ref. 8) and ω^* is calculated by

$$\omega^* = \omega_B^* \frac{\omega}{\omega_B} \qquad (17)$$

The stiffness parameter is

$$\frac{\omega_1 \ell}{V} = k \frac{\omega_1}{\omega_B} \frac{\omega_B}{\omega} \tag{18}$$

For the stiffness solution, $1/\mu$ is obtained from the assumed product $(1/\mu)\left(\omega/\omega_B\right)^2$ and the calculated ω/ω_B. The dynamic-pressure parameter is calculated according to equation (B2) of reference 8

$$\lambda \equiv \left(K_{1,1}^*\right)^4 \frac{1}{\beta} \frac{1/\mu}{\left(\omega_1 \ell/V\right)^2} \tag{19}$$

where $K_{1,1}^*$ is a function of panel-edge support and ℓ/w, and for simply supported edges it becomes

$$K_{1,1}^* = \pi \sqrt{1 + \left(\frac{\ell}{w}\right)^2} \tag{20}$$

A sufficient increase of $1/\mu$ causes g_{sf} and $g_{B,v}$ to pass from negative (indicating a stable motion) through zero (neutrally stable, or borderline flutter point) to positive values (unstable). The points with $g_{sf} = 0$ in figure 2(a) and with $g_{B,v} = 0$ in figure 2(b) are common in all respects, but they have been reached in two different planes. Figure 2(a) is in the plane $g_{B,v} = 0$, whereas figure 2(b) is in the plane $g_{i,sf} = 0$. (The latter could have been in planes $g_{i,sf}$ equal to an array of constants — possibly a different constant for each mode i — had the analyst so desired.)

There is a solution difficulty to be overcome at the static aerodynamic limit, $k = 0$, of the unsteady aerodynamic theory. In the equilibrium equations the ratio $(1/\mu)/k^2$ appears. This ratio remains finite when both k and $1/\mu$ approach zero. In order to use the same solution framework for calculating a flutter value for λ, an arbitrary non-zero value is assigned to k in the equilibrium equations while using the $\bar{Q}_{ij}$ for $k = 0$.

RESULTS AND DISCUSSION

Introductory Remarks

The effects of solid-friction and viscous structural damping are illustrated for the same panel characteristics studied above in the section "Solution Techniques," namely, simply supported edges, $\ell/w = \sqrt{0.3}$, $\Lambda = 10^\circ$, and two assumed modes in both length and width directions. Effects of solid friction alone are obtained from the flexibility solution. Effects of viscous friction and of combinations of viscous and solid-friction damping are

11

from the stiffness solution. Comparisons are shown for $k = 0$ representing the static-aerodynamic approximation, for $k = 0.01$ representing the quasi-static aerodynamic approximation, and for $k = 0.25$ representing the use of the complete unsteady aerodynamics. The majority of the studies are done with $M = 3.0$, as typical of the Mach number range where coupled-mode flutter is encountered, but one study is reported for $M = 1.3$ where "single-degree-of-freedom" flutter can be encountered.

In the "Solution Techniques" section the search procedure for finding flutter boundary points was described with plots of ω^* and g_{sf} $\left(\text{or } g_{B,v}\right)$ against λ and of stiffness parameter and g_{sf} $\left(\text{or } g_{B,v}\right)$ against $1/\mu$. The same types of plots are used in presenting the results that follow.

Comparison of Damping Effects Using the Static Aerodynamic Limit (k = 0)

It was pointed out at the end of the "Solution Techniques" section that, to obtain results for $k = 0$, the $\bar{Q}_{ij}$ are calculated for $k = 0$, but in the equilibrium equations k is assigned a nonzero value. Although any value can be assigned, $k = 0.01$ was assigned in the present work. This choice necessarily affects the range of $1/\mu$ that is selected during the search.

Solid-friction effects from a flexibility solution.- The parameter traces are shown in figure 3(a). An initial choice of $1/\mu = 0$ gives the natural-mode-in-a-vacuum points at the foot of each curve where the p,q values are labeled for reference. As $1/\mu$ is gradually increased the parameter traces move as indicated by the arrows. A small value of $1/\mu$ results in the four points indicated by the circles. The four circles fall at a constant $1/\mu$ on the plot of stiffness parameter against $1/\mu$; but on the plot of ω^* against λ the four circles fall on a parabola, and λ is a constant multiplied by $(\omega^*)^2$. For a higher chosen $1/\mu$ the four points indicated by the squares result and they fall on a lower parabola on the plot of ω^* against λ. This $1/\mu$ was chosen because two frequencies have coalesced at an instability point with $\lambda = 331$. (Two of the squares coincide at the frequency coalescence of the p,q = 2,1 and 2,2 modes.) A still higher value of $1/\mu$ gives the diamond points. The triangle points result from a yet higher value of $1/\mu$ that was selected for its closeness to the frequency coalescence of the p,q = 1,1 and 1,2 modes with $\lambda = 168$. Note that the parabola through that coalescence-point pair is tangent to the curve of ω^* against λ.

With static aerodynamics the only way a flutter instability can be reached is by a frequency coalescence, and this occurs for the present case with $\lambda = 168$, which is the flutter value.

Viscous-friction result from a stiffness solution.- The parameter traces are shown in figure 3(b) and the natural-mode values of p,q are labeled at the foot of each curve.

A small chosen value of $(1/\mu)\left(\omega/\omega_B\right)^2$ gives the parameter values indicated by the circles, and certain successively higher values give the squares, the diamonds, and the triangles. Note that each set of symbols falls on a vertical line on ω^* plotted against λ, but the symbols fall on a parabola on stiffness parameter plotted against $1/\mu$. Comparison with the flexibility-solution results in figure 3(a) reveals the contrasting behavior of any set of points (such as the circles).

On the plot of ω^* against λ the lower frequency pair of squares falls just barely above the flutter associated with frequency coalescence at $\lambda = 270$ of the modes that originate at p,q = 1,1 and 1,2, and this frequency coalescence occurs at a point of tangency with the vertical line $\lambda = 270$. The diamond points fall at an intermediate value of λ. At a higher λ a pair of the triangle points falls very nearly at the frequency coalescence of the modes originating at p,q = 2,2 and 2,1.

It is significant to observe the two different results for k = 0. From the flexibility solution with $g_{B,v} \equiv 0$ and with $\left(g_{i,sf} + g_{sf}\right)$ variable including $\rightarrow 0$, flutter occurs at a frequency coalescence at which $\lambda = 168$. (See fig. 3(a).) From the stiffness solution with $g_{i,sf} = g_{sf} \equiv 0$ and with $g_{B,v}$ variable including $g_{B,v} \rightarrow 0$, frequency-coalescence flutter occurs at a frequency coalescence with $\lambda = 270$. This finding is discussed further subsequently.

Viscous-plus-solid-friction result from stiffness solution.- In order to study combined effects of viscous and solid friction, especially for small amouts of solid-friction damping, $g_{i,sf}$ was set equal to 0.01 (all modes). The results from a stiffness solution are shown in figure 3(c). At the crossing point $g_{B,v} = 0$, the same result is obtained ($\lambda = 168$) as from the flexibility solution with $g_{B,v} \equiv 0$ and $g_{sf} = 0.01$ as shown in figure 3(a). Small increments of $g_{B,v}$ above 0 are strongly stabilizing. For $g_{B,v} = 0.001$, $\lambda = 176$; and for $g_{B,v} = 0.01$, $\lambda = 229$.

A separate solution for $g_{i,sf} = 0.001$ was made in order to approach more closely the limit $g_{i,sf} \rightarrow 0$. The flutter λ was again 168, and increase of $g_{B,v}$ was even more strongly stabilizing than in the presence of $g_{i,sf} = 0.01$.

Although such solutions that are very close to $g_{i,sf} \equiv 0$ do not constitute a formal mathematical proof of the limiting value of λ, it is strongly believed that $\lambda = 168$ is the limit value as $g_{i,sf} \rightarrow 0$ within the stiffness solution because of the smooth and regular behavior of all the forces acting.

Summary plot of effects of solid-friction and viscous damping.- Figure 4 represents a three-dimensional plot of λ against both $g_{B,v}$ and $\left(g_{i,sf} + g_{sf}\right)$. The curve segments in the three planes $g_{B,v} = 0$, $g_{i,sf} = 0$, and $g_{i,sf} = 0.01$ are from figures 3(a), 3(b), and 3(c), respectively. The discontinuous result for λ for $g_{sf} \rightarrow 0$ compared with $g_{sf} \equiv 0$ is shown.

Comparison of Damping Effects Using Quasi-Static

Aerodynamics (k = 0.01)

A very low value of k (0.01) is used in order to study the damping effects in the vicinity of the limit $k \to 0$, where the quasi-static aerodynamic approximation is most valid.

Solid-friction effects from a flexibility solution.- The parameter traces are shown in figure 5(a) and, being from the flexibility solution, are for the condition (and in the plane) $g_{B,v} \equiv 0$. In order to display better the pertinent trace behavior, the range of the g_{sf} scale is between ±0.02, which is much less than in figures 2 and 3. The points on the traces at certain successively higher $1/\mu$ values indicated by the circles, squares, diamonds, and triangles are at the same $1/\mu$ values as in figure 3(a). The trace or mode that reaches the flutter point is the one originating at $p,q = 1,2$, and for $g_{sf} > 0$ the curves on all figure parts are a series of dots for the purpose of identification. At the crossing point $g_{sf} = 0$, $\lambda = 270$. For $g_{sf} = 0.01$, λ drops sharply to 215 indicating the strong destabilizing effect of solid friction in this parameter range. (The other trace that reaches an instability at a higher λ originates at $p,q = 2,2$, and for $g_{sf} > 0$ it is identified by a row of x's on each figure part.)

Viscous-friction result from stiffness solution.- The parameter traces for $g_{i,sf} = 0$ are shown in figure 5(b). The range of $g_{B,v}$ is restored to ±0.4 in order to display better the trace behavior. At the crossing point $g_{B,v} = 0$, $\lambda = 270$. For a small or even substantial increase in $g_{B,v}$ the increase in λ is insignificantly small.

Viscous-plus-solid-friction result from a stiffness solution.- Values of $g_{i,sf}$ for all indexes i are set equal to 0.01, the same as for $k = 0$ described previously, and the results are shown in figure 5(c). At the crossing point $g_{B,v} = 0$, $\lambda = 215$ which is the same as for $g_{sf} = 0.01$ in figure 5(a), as it should be, since they are a common point reached in two different intersecting solution surfaces. An increase of $g_{B,v}$ above 0 is stabilizing: for $g_{B,v} = 0.01$, $\lambda = 236$.

Summary plot of effects of solid-friction and viscous damping.- Figure 6 represents a three-dimensional plot of λ against both $g_{B,v}$ and $\left(g_{i,sf} + g_{sf} \right)$. In comparison to figure 4 with $k = 0$, here the discontinuous behavior has disappeared and there is a steep negative slope with varying $\left(g_{i,sf} + g_{sf} \right)$. The curves in the three planes $g_{B,v} = 0$, $g_{i,sf} = 0$, and $g_{i,sf} = 0.01$ are from figures 5(a), 5(b), and 5(c), respectively.

Although a formal mathematical proof is lacking, it is concluded that there is a discontinuous result for λ from the flexibility solution for $k \to 0$; namely, for $g_{i,sf} + g_{sf} = 0$, $\lambda = 168$ for $k \equiv 0$, but $\lambda = 270$ for $k \to 0$. This conclusion is reached because of the smooth and regular behavior of the aerodynamic forces in the vicinity of

k → 0 and from observation of how an instability (flutter) point is reached in the solution processes.

Comparison of Damping Effects Using
Complete Unsteady Aerodynamics

A result of using the complete unsteady aerodynamic theory is shown in figures 2(a) and 2(b) for $k = 0.25$. This figure was used earlier to illustrate the technique of solution. The flutter point with $\lambda = 293$ is at the crossing point $g_{sf} = 0$ in figure 2(a) and at the crossing point $g_{B,v} = 0$ in figure 2(b). An increase of g_{sf} to 0.02 predicts a small decrease of λ to 286. An increase of $g_{B,v}$ to 0.02 predicts a small increase of λ to 302.

At the common point, $g_{sf} = g_{B,v} = 0$, $\lambda = 293$, $1/\mu = 0.0721$, $\omega_1 \ell/V = 0.1196$, and the product $(1/\mu)(\omega_1 \ell/V) = 0.00862$. Figure 7 shows a flutter boundary in the plane $1/\mu$ plotted against stiffness parameter $\omega_1 \ell/V$ as used in reference 3 and in subsequent publications. The solution points for $k = 0.25$ and 0.01 discussed previously are indicated. A variable thickness of panel with a fixed panel material, altitude, and Mach number determines a hyperbola $(1/\mu)(\omega_1 \ell/V) =$ Constant. The hyperbola of short dashes is for aluminum at standard sea level and with $M = 3$, for which $(1/\mu)(\omega_1 \ell/V) = 0.00851$. Increasing thickness is to the right toward the stable region. The intersection of the hyperbola with the flutter boundary determines the thickness ratio required to prevent flutter.

For panel and flow parameters that result in a flutter boundary characterized by a slow variation of λ and of ω/ω_B with varying k and altitude, extrapolations and interpolations to obtain additional points on a flutter boundary can be obtained on the basis of assumed constant λ and ω/ω_B. The associated proportionalities are

$$\lambda \propto \frac{1/\mu}{(\omega_1 \ell/V)^2} = \frac{(1/\mu)(\omega_1 \ell/V)}{(\omega_1 \ell/V)^3} \propto \frac{(1/\mu)(\omega_1 \ell/V)}{k^3} \qquad (21)$$

from which

$$k \propto \left(\frac{1}{\mu} \frac{\omega_1 \ell}{V} \right)^{1/3} \qquad (22)$$

When an analyst has tried a value of k and obtained a point on a flutter boundary that does not fall on a desired hyperbola of panel material and altitude, he can estimate his next value of k from equation (22).

15

Comparison of Damping Effects at M = 1.3

All of the results discussed previously are for M = 3.0, as representative of a Mach number well above any transonic or low supersonic effects. In this higher range of M, panel flutter is characterized by strong coupling of the assumed deflection modes used in a modal analysis. In the low supersonic range, for M less than about $\sqrt{2}$, and for panels with ℓ/w less than about 2 to 4, a different type of flutter is predicted. The flutter motion is dominated by a single mode and is often termed "single-degree-of-freedom flutter," although the other modes are present in small proportions.

Results calculated for the same panel discussed previously, but with M = 1.3, are presented in figure 8. As indicated by the key and the labels, the solid boundary on the right is the flutter boundary for $g_{B,v} = g_{sf} = 0$. For all the lower part of that boundary the flutter motion is predominantly the p,q = 2,1 mode. An increase of viscous damping alone to $g_{B,v} = 0.01$ has a significant stabilizing effect by shrinking the flutter region to within the boundary of short dashes. An increase of solid-friction damping alone has a comparatively greater stabilizing effect by shrinking the flutter region to within the boundary of long and short dashes. The solid, nearly parabolic-shaped boundary to the left is an instability boundary characterized by strong modal coupling, and it is little affected by structural damping except close to the origin where k is very small. A sufficient increase of $g_{B,v}$ and/or g_{sf} shrinks the flutter region that is dominated by the single-degree-of-freedom (p,q = 2,1) mode, until the coupled-mode instability boundary becomes the flutter boundary.

Comments on Convergence With Respect to the
Number of Modes in the Modal Analysis

All of the results of the present report were determined by using four modes in the Galerkin modal analysis — two modes lengthwise and two widthwise even though these results are not particularly well converged. The use of four modes in both directions gives a λ roughly 30 percent higher, and it was established that this four-by-four-mode result is well converged, at least for $\Lambda = 0^{\circ}$ and 90°. The effects of solid-friction and viscous structural damping are the primary subject of this report, and these effects are the same from the two-by-two-mode results and from the four-by-four-mode results. The 16-mode results are so much more complicated to present and describe that the decision was made to present the 4-mode results.

Review of Results

The two types of structural damping, solid friction and viscous, are shown to have mostly contrasting effects on panel-flutter boundaries for the panel and flow parameters

investigated. Solid-friction damping is strongly to moderately destabilizing, whereas viscous damping is stabilizing or ineffective. This stabilizing effect of viscous damping on panels contrasts with the findings of Ellen in reference 7 for two-dimensional membranes based on quasi-static aerodynamics. Figure 1(b) of reference 7 shows a marked destabilizing effect of both viscous and solid-friction (i.e., hysteretic) damping. Since the effects of the two types of structural damping are found to be so different herein, there cannot be an "equivalent viscous damping" for solid-friction structural damping in panel flutter.

Flutter solutions were obtained for a particular yawed panel for $M = 3.0$. With use of the static-aerodynamic approximation ($k = 0$), the stiffness solution gives a discontinuous result for λ in the vicinity of $g_{i,sf} \approx 0$ in the plane $g_{B,v} = 0$. For $g_{i,sf} \equiv 0$, $\lambda = 270$; but for $g_{i,sf} \to 0$, $\lambda = 168$. Another discontinuous result is obtained from the flexibility solution in the vicinity $k \approx 0$ for $g_{sf} \equiv g_{B,v} \equiv 0$. For $k \equiv 0$ (i.e., static aerodynamics), $\lambda = 168$; but for $k \to 0$ (i.e., quasi-static aerodynamics), $\lambda = 270$.

The complete unsteady aerodynamic forces were used for $k = 0.25$ in order to calculate a point on the flutter boundary that corresponds to aluminum panels at sea level. All of the flutter boundary results for $M = 3$ are characterized by a flutter motion of strongly coupled assumed deflection modes.

The low Mach number region was studied for the same panel with $M = 1.3$. Here, the flutter boundary is characterized for low structural damping by a flutter motion that is dominated by just one of the assumed modes ("single-degree-of-freedom flutter" herein termed "DOF"). This single DOF boundary is not at all characterized by a nearly constant λ. Addition of both solid-friction and viscous damping is strongly stabilizing, and a sufficient increase of either type of damping rapidly shrinks the single DOF flutter region until a coupled-mode flutter boundary is encountered. This latter boundary is like the coupled-mode boundary for $M = 3$ in that λ varies slowly with $1/\mu$, and the boundary is little affected by further increases in damping, except at very low $1/\mu$.

CONCLUSIONS

An equilibrium equation has been given that accounts for both solid-friction and viscous structural damping in panel-flutter analysis. A solution technique has been developed for routinely calculating the effects of both types separately and in combination. The solution technique is usable with aerodynamic forces from general unsteady potential flow. A Galerkin modal analysis of a rectangular yawed panel at two Mach numbers M of 3.0 and 1.3 leads to the following conclusions:

1. The additions of solid-friction and viscous structural damping to the panel have opposing effects on the coupled-mode flutter boundary: solid-friction damping is mostly destabilizing, but viscous damping is stabilizing or ineffective in every case investigated.

The relative effects of structural damping are the greatest at the lowest mass ratios (air mass to panel mass) and become smaller as mass ratio increases.

2. Since the two types of damping result in opposing effects at $M = 3.0$, there cannot be, in general, an "equivalent viscous" damping to solid-friction damping.

3. Two discontinuous results for flutter dynamic-pressure parameter are obtained at $M = 3.0$ in the vicinity of reduced frequency $k \approx 0$ and in the vicinity of solid-friction damping $g_{sf} \approx 0$.

4. At a low supersonic Mach number, $M = 1.3$, the flutter boundary is a "single-degree-of-freedom" flutter boundary for the important range of mass ratios and for low structural damping. Both types of damping are strongly stabilizing for the single-degree-of-freedom flutter. A sufficient increase of structural damping shrinks the single-degree-of-freedom flutter region until a coupled-mode flutter boundary is encountered, for which the structural damping effects are similar to those for $M = 3.0$.

Langley Research Center
National Aeronautics and Space Administration
Hampton, VA 23665
August 2, 1976

APPENDIX

GENERALIZED AERODYNAMIC-FORCE ELEMENTS Q_{ij}

The generalized aerodynamic-force element is, as given by equation (11),

$$Q_{ij} \equiv \ell w \iint_S \Delta p_j h_i \, d\bar{x} \, d\bar{y} \tag{A1}$$

The lifting-pressure difference Δp_j is that from the modal series of equation (8)

$$\Delta p(\bar{x}, \bar{y}, \tau) \approx e^{i\omega\tau} \sum_j \frac{q_j}{\ell} \Delta p_j(\bar{x}, \bar{y}) \tag{A2}$$

The lifting pressure is obtained from the perturbation velocity potential $\varphi(\bar{x}, \bar{y}, \tau)$ by

$$\Delta p(\bar{x}, \bar{y}, \tau) = -\rho \, \frac{d\varphi(\bar{x}, \bar{y}, \tau)}{d\tau} \tag{A3}$$

By using a modal series for φ that is consistent with the series for Δp and for deflection z,

$$\varphi(\bar{x}, \bar{y}, \tau) \approx \sum_j \frac{q_j}{\ell} \varphi_j(\bar{x}, \bar{y}) e^{i\omega\tau} \tag{A4}$$

and

$$\Delta p(\bar{x}, \bar{y}, \tau) = -\rho V e^{i\omega\tau} \sum_j \frac{q_j}{\ell} \left(\cos \Lambda \, \frac{\partial \varphi_j}{\partial(\ell \bar{x})} + \sin \Lambda \, \frac{\partial \varphi_j}{\partial(w\bar{y})} + i \, \frac{\omega}{V} \, \varphi_j \right) \tag{A5}$$

which gives for the individual Δp_j

$$\Delta p_j = -\rho V \left(\cos \Lambda \, \frac{\partial \varphi_j}{\partial(\ell \bar{x})} + \sin \Lambda \, \frac{\partial \varphi_j}{\partial(w\bar{y})} + i \, \frac{\omega}{V} \, \varphi_j \right) \tag{A6}$$

19

APPENDIX

where

$$\varphi_j\left(\bar{x}(x,y),\bar{y}(x,y)\right) = \frac{V}{\pi} \iint\limits_{S^*} \frac{w_j(\xi,\eta)}{V} \frac{e^{-i\bar{\omega}(x-\xi)} \cos\left(\frac{\bar{\omega}}{M} R\right)}{R} d\xi \, d\eta \tag{A7}$$

wherein:

S^* region of integration, the panel area within the forward-facing Mach characteristic cone with apex at x,y

x,y   streamwise and cross-stream dimensional coordinates, respectively, with same origin as $\bar{x},\bar{y}$:

$$x = \ell\bar{x} \cos \Lambda + w\bar{y} \sin \Lambda$$

$$y = w\bar{y} \cos \Lambda - \ell\bar{x} \sin \Lambda$$

ξ,η dummy variables for x,y, respectively

R $= \sqrt{(x - \xi)^2 - \beta^2(y - \eta)^2}$

$\bar{\omega}$ $= \dfrac{M^2\omega}{\beta^2 V}$

and the downwash amplitude is

$$w_j = V\left(\cos \Lambda \frac{\partial h_i}{\partial\bar{x}} + \frac{\ell}{w} \sin \Lambda \frac{\partial h_i}{\partial\bar{y}} + i \frac{\omega\ell}{V} h_i\right)$$

Substitution of equation (A6) into equation (A1) gives

$$Q_{ij} = \frac{-\rho V}{\ell} \iint\limits_{S} h_i\left(\cos \Lambda \frac{\partial \varphi_j}{\partial\bar{x}} + \frac{\ell}{w} \sin \Lambda \frac{\partial \varphi_j}{\partial\bar{y}} + i \frac{\omega\ell}{V} \varphi_j\right) d\left(\ell\bar{x}\right) d\left(w\bar{y}\right) \tag{A8}$$

APPENDIX

Integration by parts of the terms that involve $\sin \Lambda$ and $\cos \Lambda$ yields

$$Q_{ij} = -\rho V w \left[\int_{\bar{y}=0}^{1} \cos \Lambda \left(h_i \varphi_j \Big|_{\bar{x}=0}^{\bar{x}=1} - \int_{\bar{x}=0}^{1} \frac{\partial h_i}{\partial \bar{x}} \varphi_j \, d\bar{x} \right) d\bar{y} \right.$$

$$+ \int_{\bar{x}=0}^{1} \frac{\ell}{w} \sin \Lambda \left(h_i \varphi_j \Big|_{\bar{y}=0}^{\bar{y}=1} - \int_{\bar{y}=0}^{1} \frac{\partial h_i}{\partial \bar{y}} \varphi_j \, d\bar{y} \right) d\bar{x}$$

$$\left. + \int_0^1 \int_0^1 i \frac{\omega \ell}{V} h_i \varphi_j \, d\bar{x} \, d\bar{y} \right] \tag{A9}$$

Where panel edges can displace vertically, the terms $h_i \varphi_j$ evaluated at those edges can be significant; but for the usual situation of $h_i = 0$ at the edges, Q_{ij} is determined by the remaining terms

$$Q_{ij} = \rho V w \int_0^1 \int_0^1 \left(\cos \Lambda \frac{\partial h_i}{\partial \bar{x}} + \frac{\ell}{w} \sin \Lambda \frac{\partial h_i}{\partial \bar{y}} - i \frac{\omega \ell}{V} h_i \right) \varphi_j \, d\bar{x} \, d\bar{y}$$

$$= \rho V w \int_0^1 \int_0^1 \left(w_i^*/V \right) \varphi_j \, d\bar{x} \, d\bar{y} \tag{A10}$$

where the velocity potential φ_j is that of equation (A7) and w_i^*/V is the complex conjugate of the downwash ratio w_i/V. (Compare with w_j of eq. (A7).) The elements Q_{ij} as given in equation (A10) are used in the present report.

REFERENCES

1. Neumark, S.: Concept of Complex Stiffness Applied to Problems of Oscillations With Viscous and Hysteretic Damping. R. & M. No. 3269, British A.R.C., 1962.

2. Hedgepeth, John M.; Budiansky, Bernard; and Leonard, Robert W.: Analysis of Flutter in Compressible Flow of a Panel on Many Supports. J. Aero. Sci., vol. 21, no. 7, July 1954, pp. 475-486.

3. Nelson, Herbert C.; and Cunningham, Herbert J.: Theoretical Investigation of Flutter of Two-Dimensional Flat Panels With One Surface Exposed to Supersonic Potential Flow. NACA Rep. 1280, 1956. (Supersedes NACA TN 3465.)

4. Theodorsen, Theodore; and Garrick, I. E.: Mechanism of Flutter − A Theoretical and Experimental Investigation of the Flutter Problem. NACA Rep. 685, 1940.

5. Johns, D. J.; and Parks, P. C.: Effect of Structural Damping on Panel Flutter. Aircraft Eng., vol. XXXII, no. 380, Oct. 1960, pp. 304-308.

6. Dugundji, John: Theoretical Considerations of Panel Flutter at High Supersonic Mach Numbers. AIAA J., vol. 4, no. 7, July 1966, pp. 1257-1266.

7. Ellen, C. H.: Influence of Structural Damping on Panel Flutter. AIAA J., vol. 6, no. 11, Nov. 1968, pp. 2169-2174.

8. Cunningham, Herbert J.: Flutter Analysis of Flat Rectangular Panels Based on Three-Dimensional Supersonic Unsteady Potential Flow. NASA TR R-256, 1967.
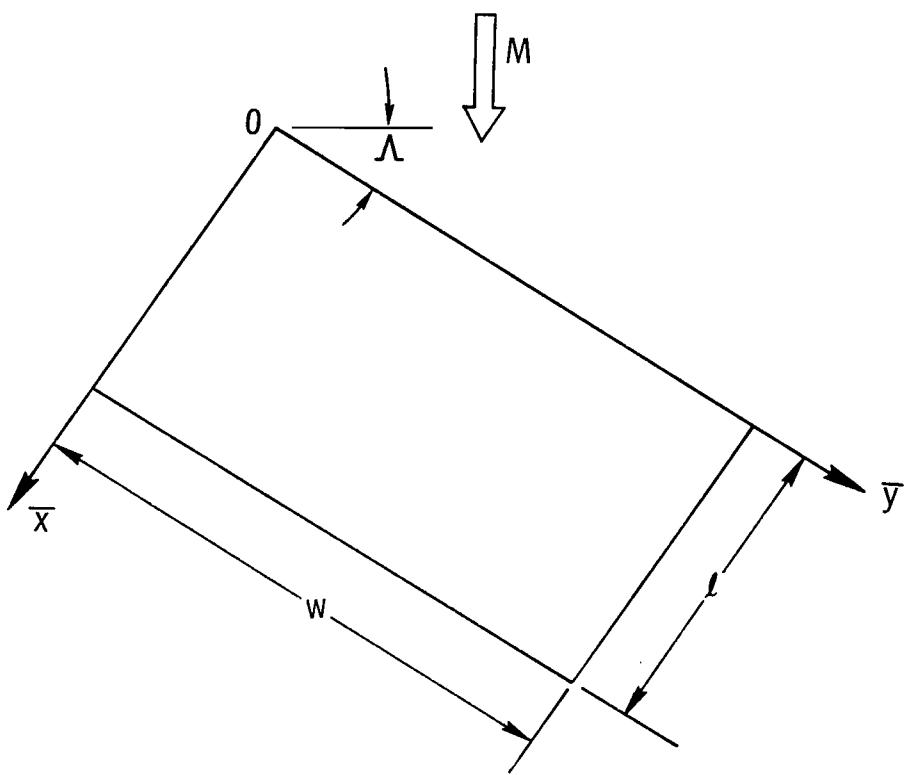
Figure 1.- Yawed panel and its coordinate system.
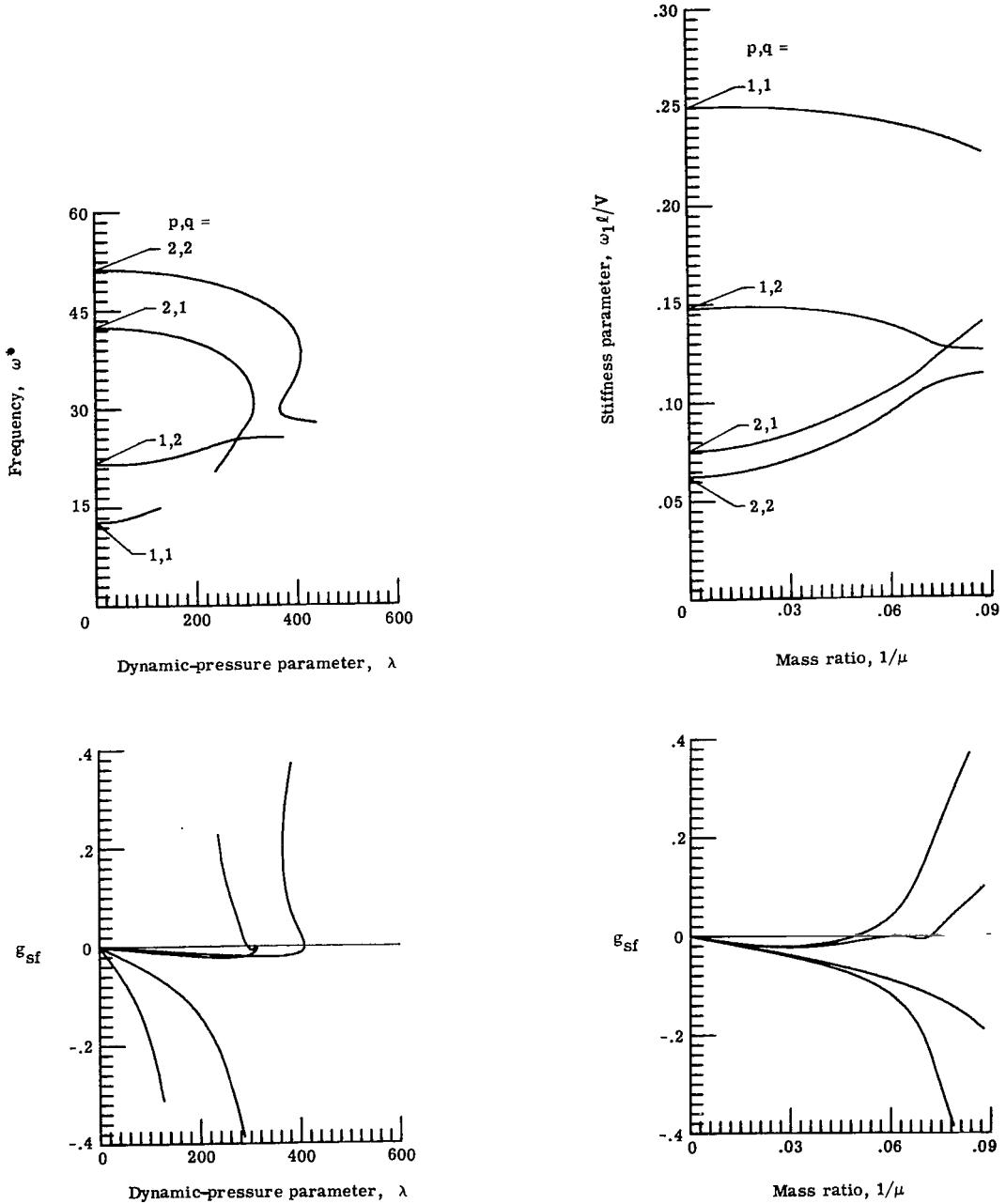
(a) Flexibility solution.

Figure 2.- Parameter traces from flutter solution for panel with $\ell/w = \sqrt{0.3}$, $\Lambda = 10^O$, $M = 3.0$, and $k = 0.25$.

24
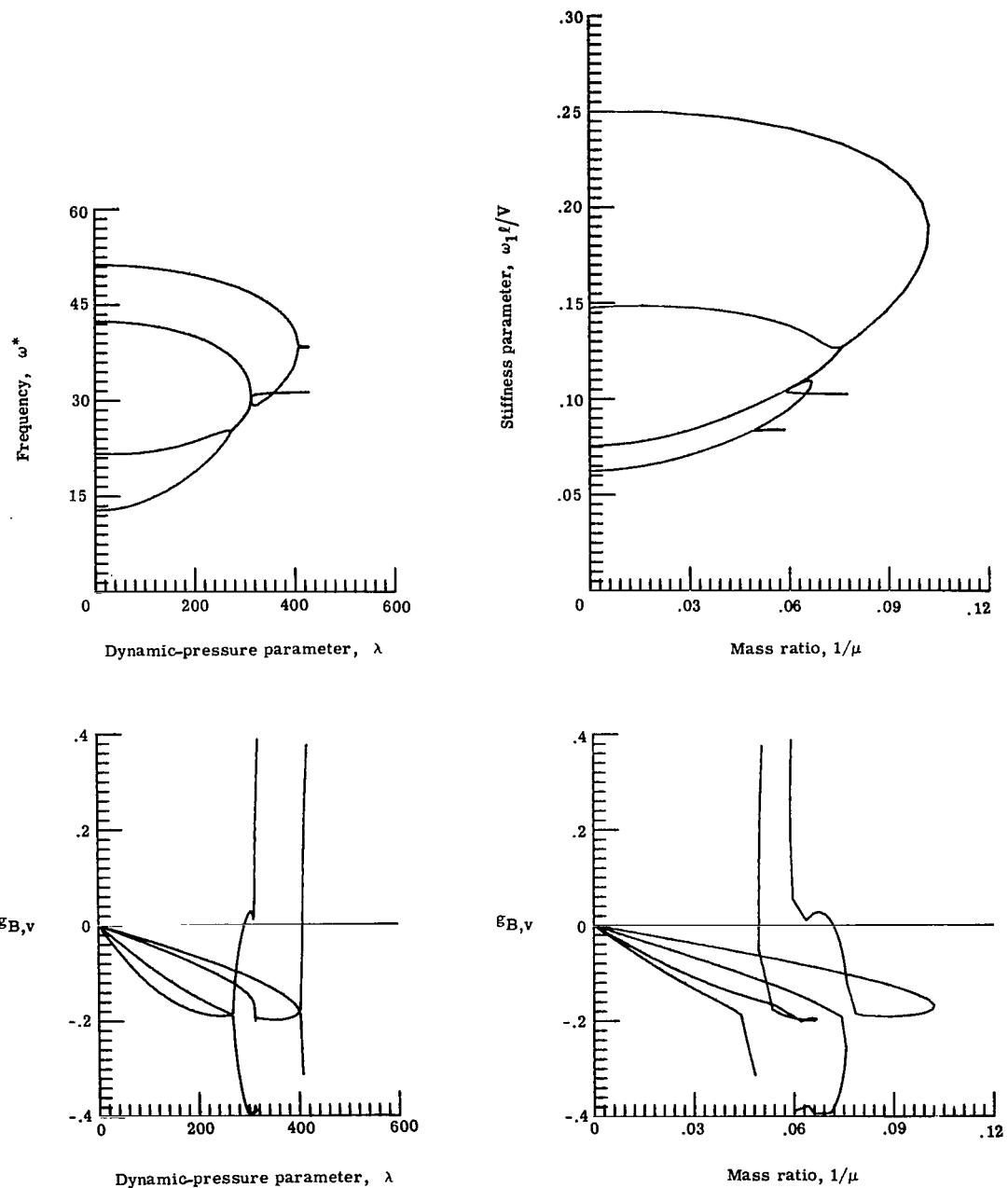
(b) Stiffness solution.

Figure 2.- Concluded.
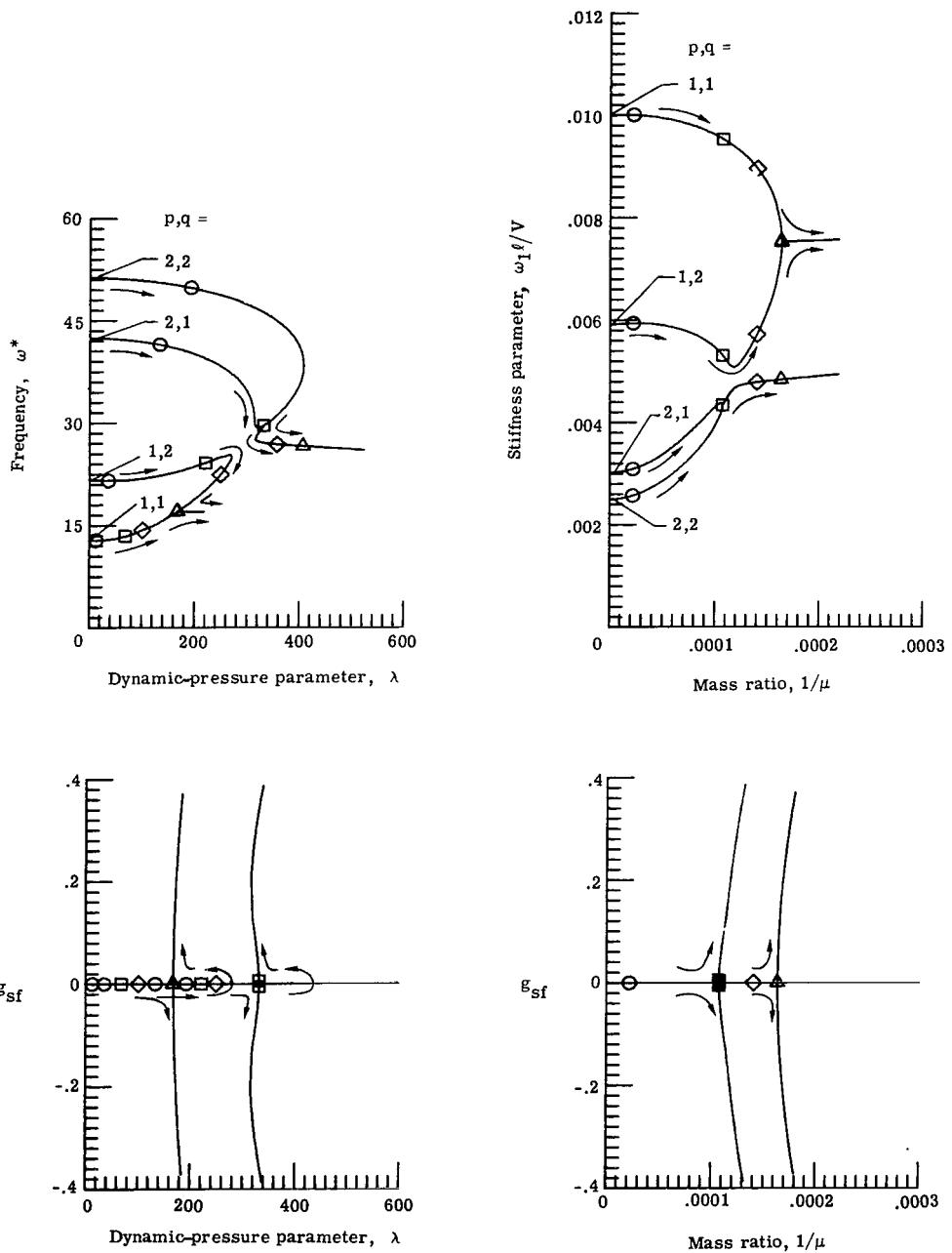
(a) Flexibility solution. $g_{i,sf} = 0$.

Figure 3.- Parameter traces from flutter solution for panel with $\ell/w = \sqrt{0.3}$, $\Lambda = 10^{O}$, $M = 3.0$, and $k = 0$.

26
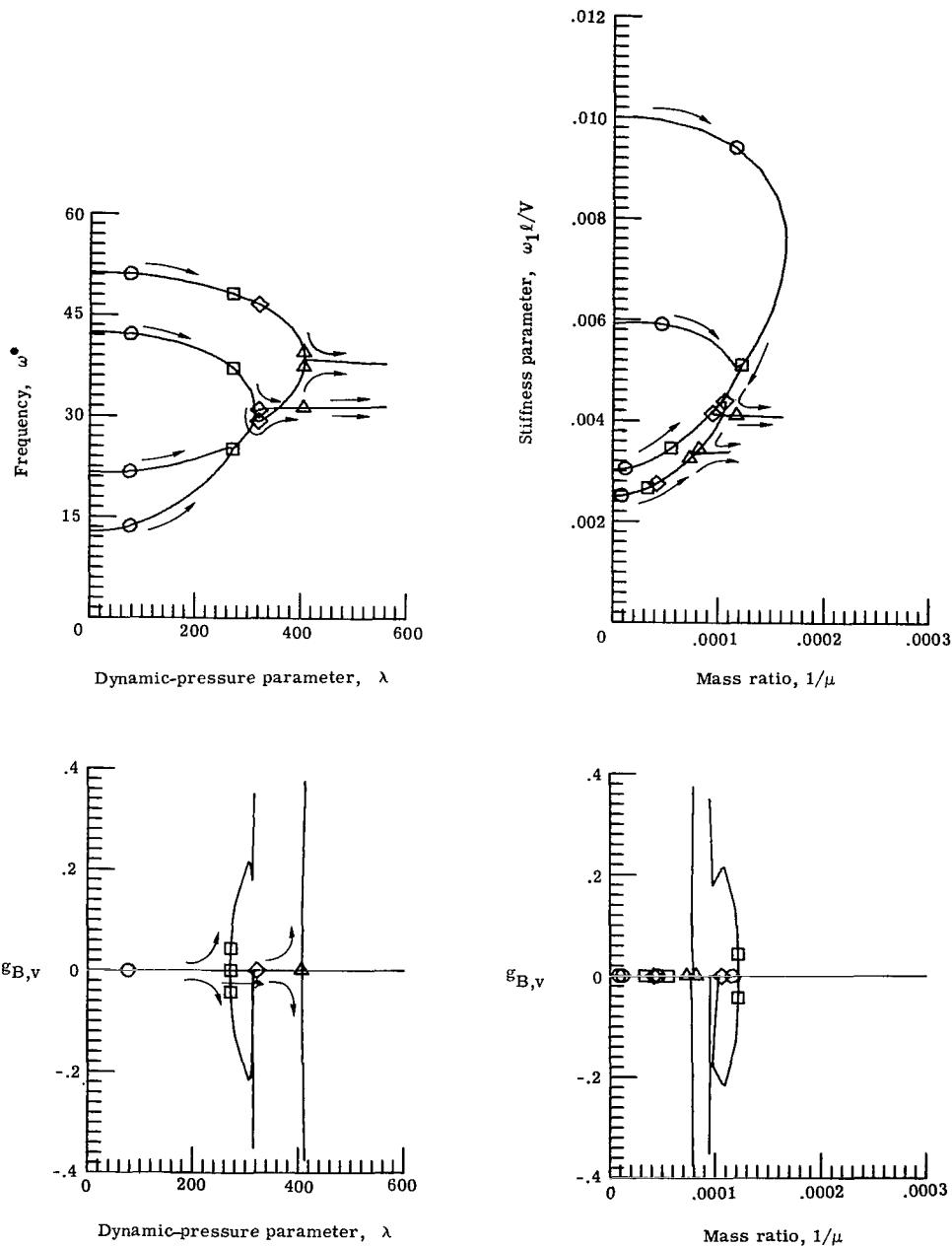
(b) Stiffness solution. $g_{i,sf} = 0$.

Figure 3.- Continued.

27
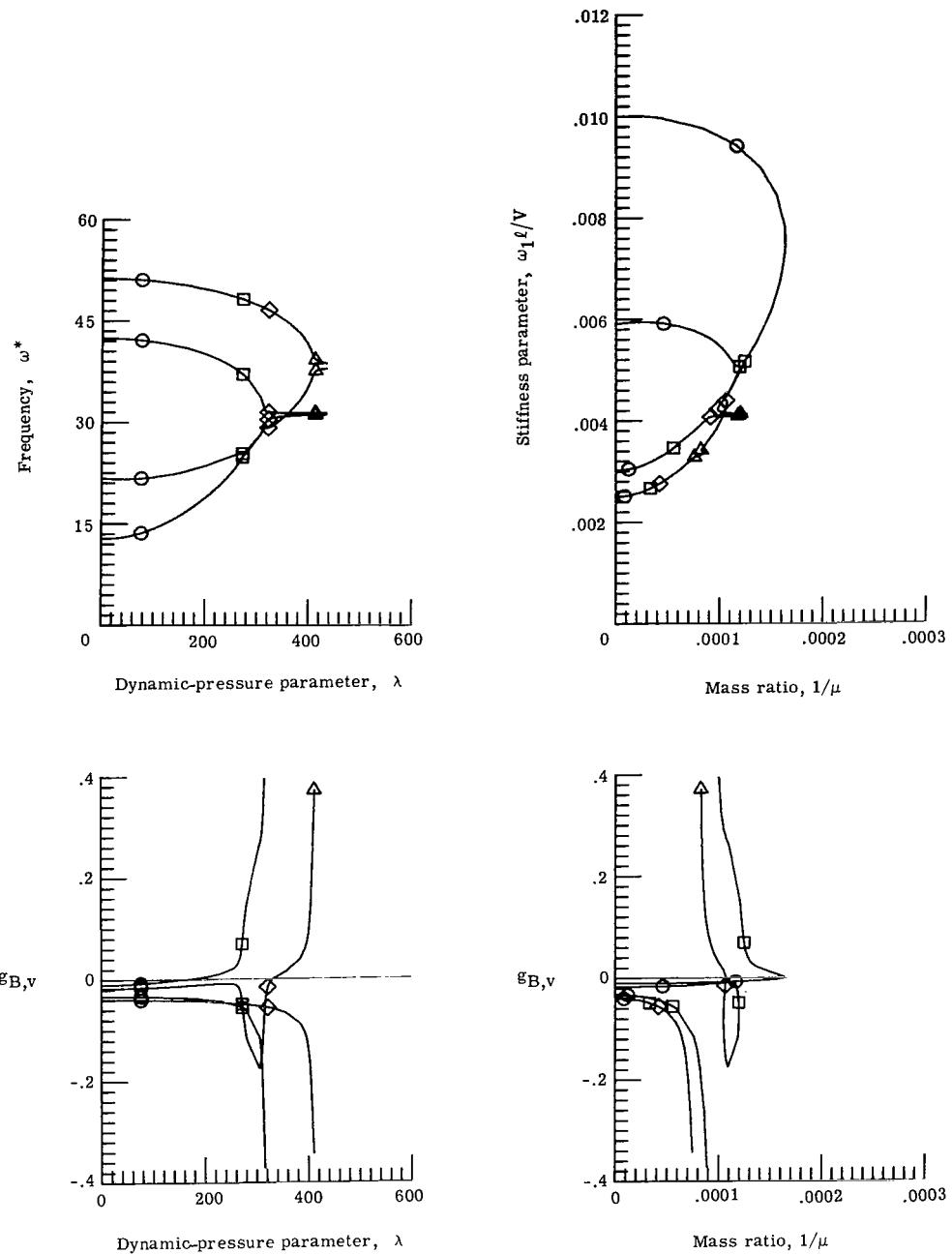
(c) Stiffness solution. $g_{i,sf} = 0.01$.

Figure 3.- Concluded.
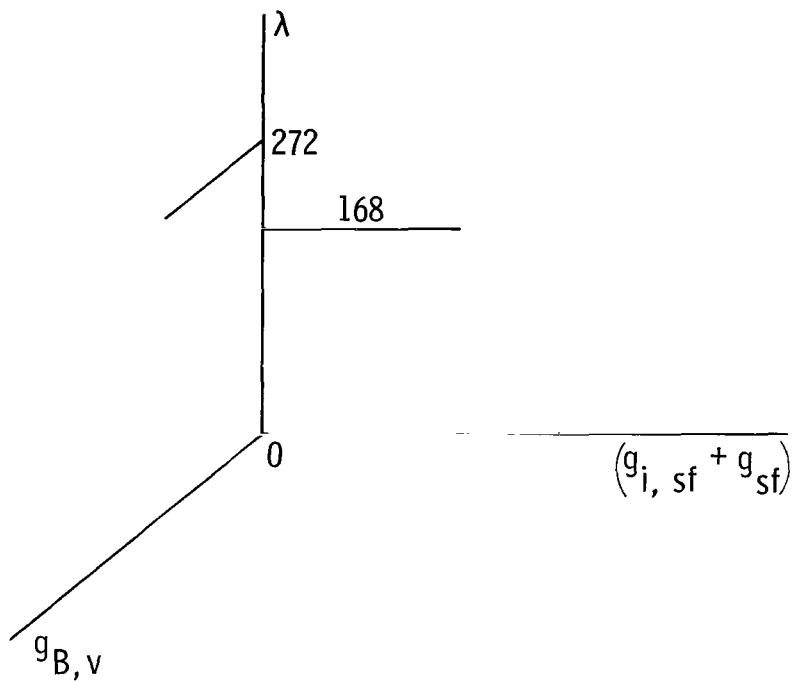
Figure 4.- Dynamic-pressure parameter λ against g_{sf} with $g_{B,v} = 0$, and against $g_{B,v}$ with $g_{sf} = 0$ for panel with $\ell/w = \sqrt{0.3}$, $\Lambda = 10^{\circ}$, $M = 3.0$, and $k = 0$.
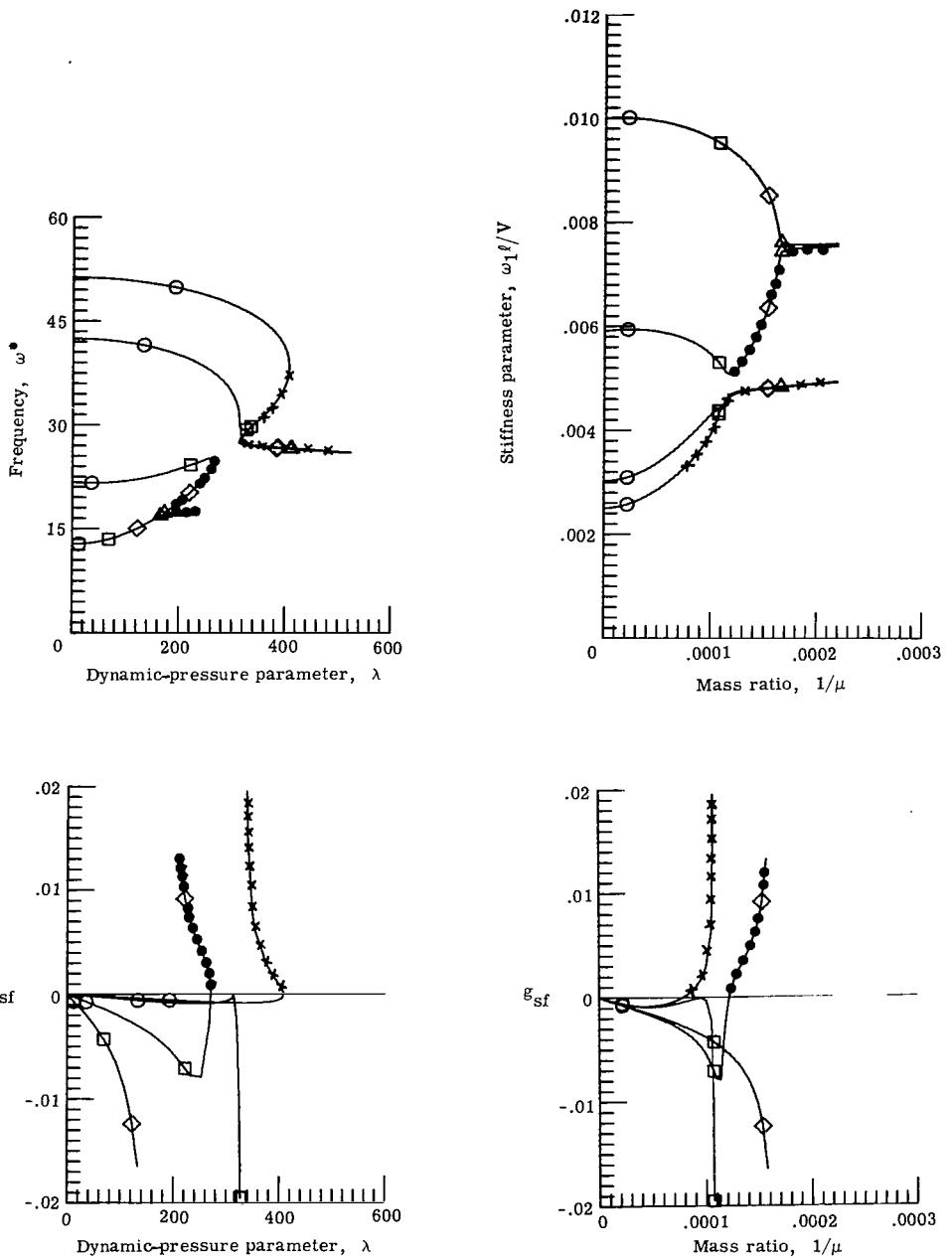
(a) Flexibility solution. $g_{i,sf} = 0$.

Figure 5.- Parameter traces from flutter solution for panel with $\ell/w = \sqrt{0.3}$, $\Lambda = 10^{O}$, $M = 3.0$, and $k = 0.01$.
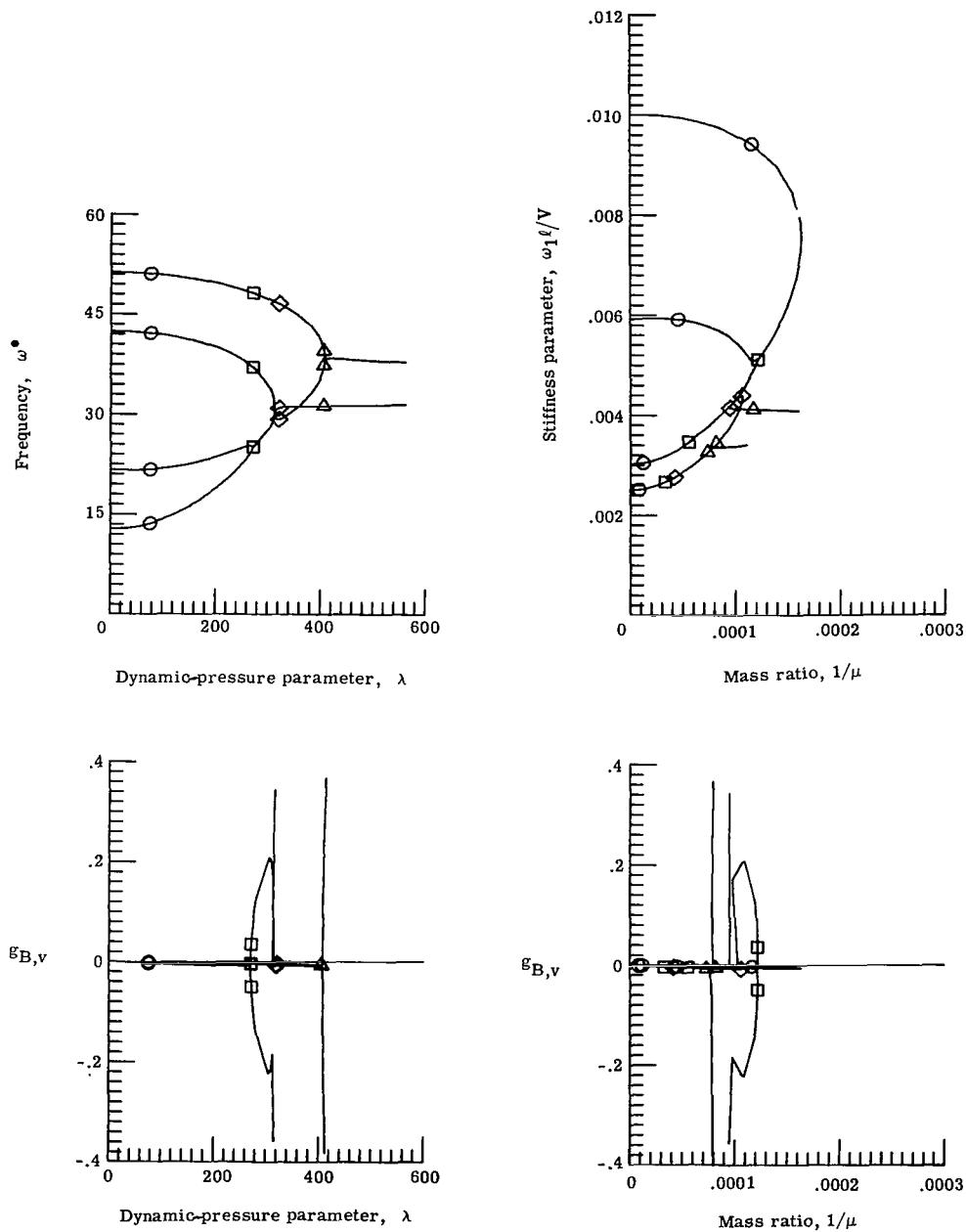
(b) Stiffness solution. $g_{i,sf} = 0$.

Figure 5.- Continued.
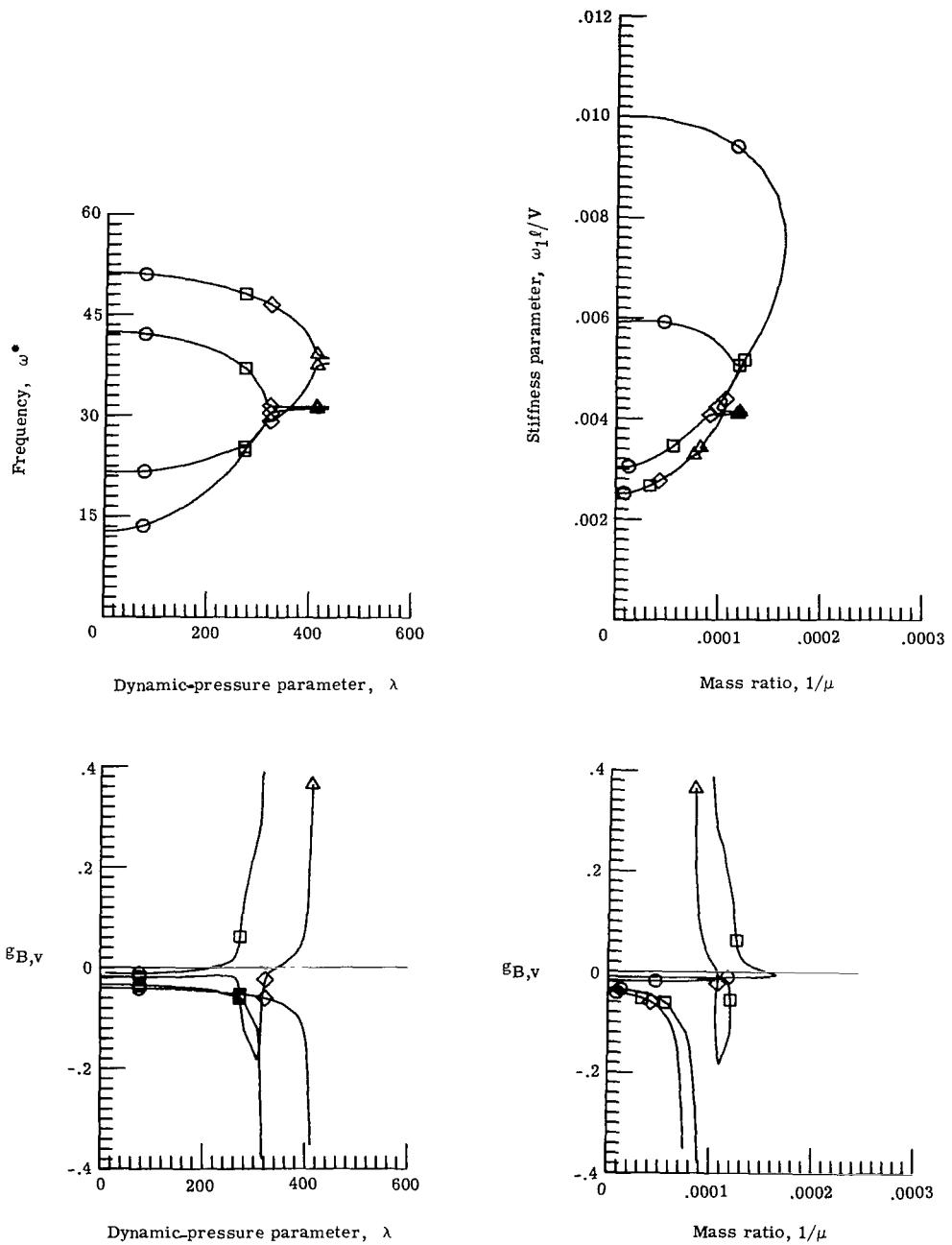
(c) Stiffness solution. $g_{i,sf} = 0.01$.

Figure 5.- Concluded.
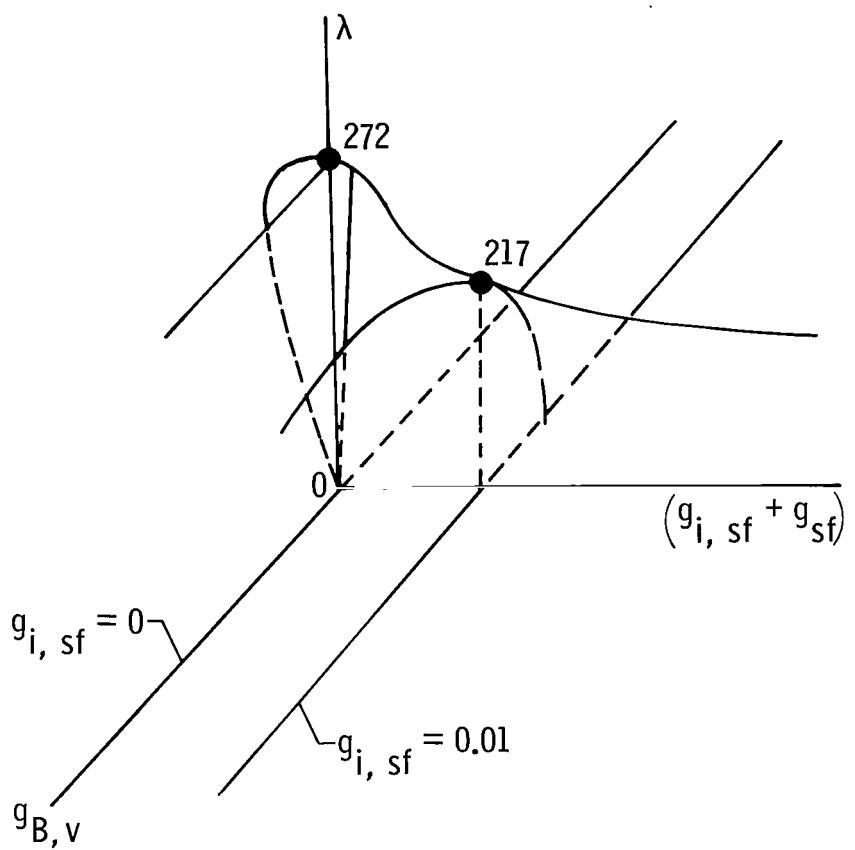
Figure 6.- Dynamic-pressure parameter λ against $\left(g_{i,sf} + g_{sf}\right)$ with $g_{B,v} = 0$, and against $g_{B,v}$ with $g_{i,sf} = 0$ and 0.01 for panel with $\ell/w = \sqrt{0.3}$, $\Lambda = 10^{\circ}$, $M = 3.0$, and $k = 0.01$.
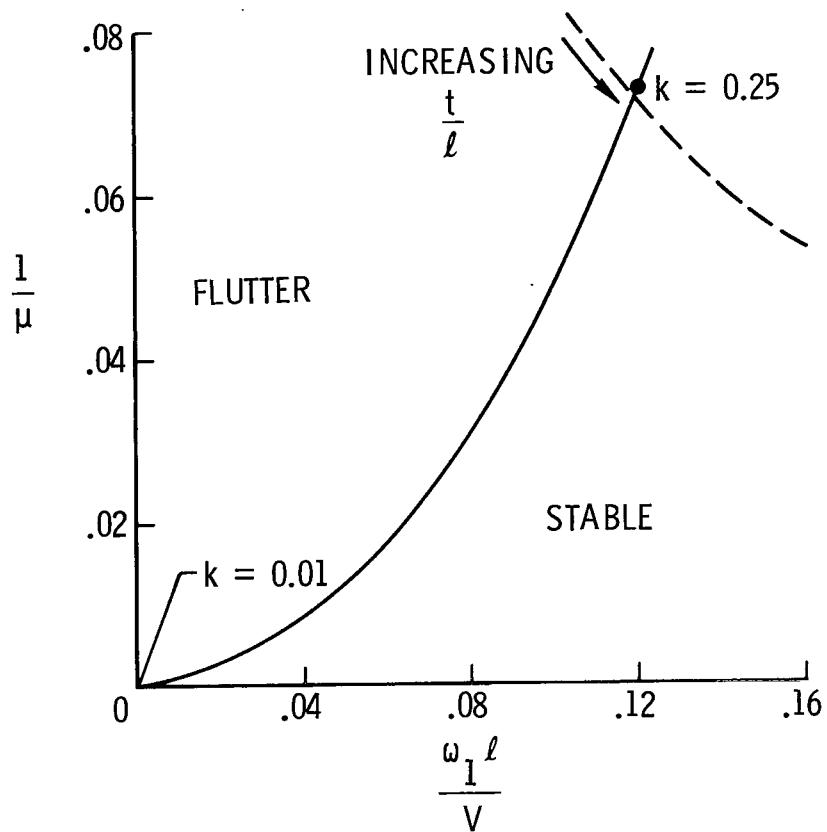
Figure 7.- Flutter boundary. Mass ratio $1/\mu$ against stiffness parameter $\omega_1 \ell/V$ for panel with $\ell/w = \sqrt{0.3}$, $\Lambda = 10^o$, $g_{i,sf} = 0$, and $M = 3$.
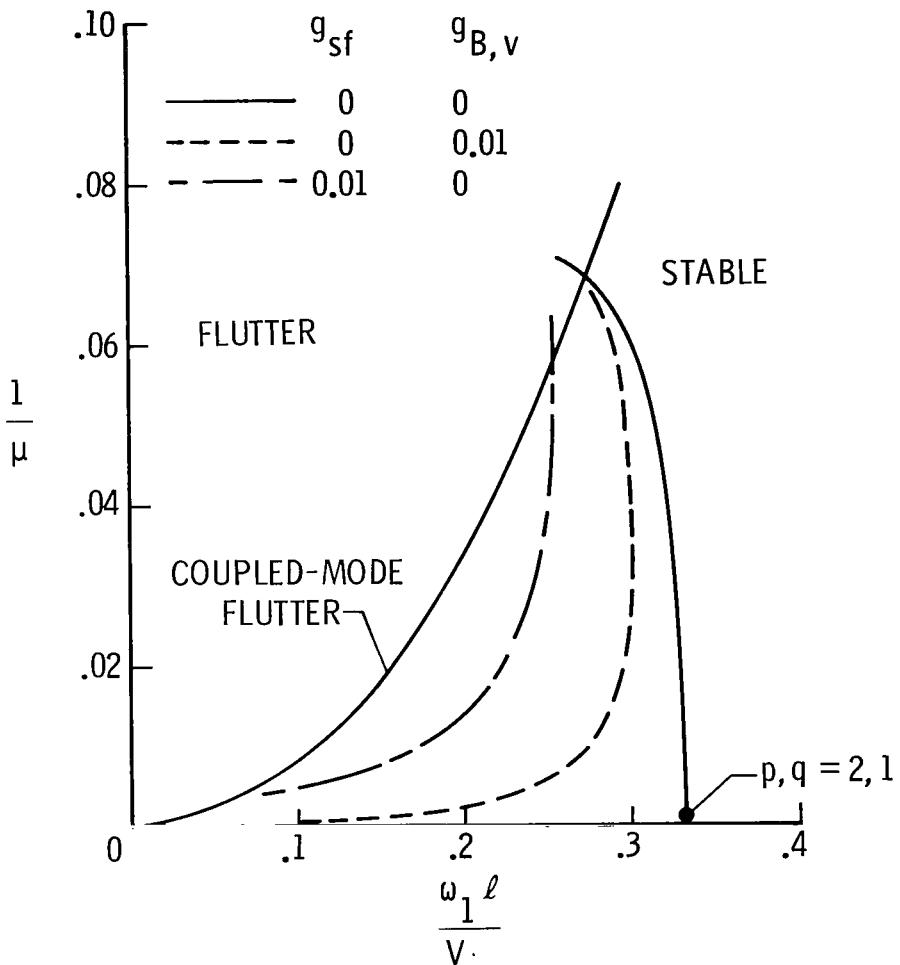
Figure 8.- Flutter boundary. Mass ratio $1/\mu$ plotted against stiffness parameter $\omega_1 \ell / V$ for panel with $\ell/w = \sqrt{0.3}$, $\Lambda = 10^\circ$, and $M = 1.3$.